International Journal of Nanomedicine

Dovepress
Taylor & Francis Group

Open Access Full Text Article

ORIGINAL RESEARCH

# Construction of Active-Passive Dual-Targeted Drug-Loaded Micelle Nanoparticles with Modified Dopamine Molecules for Efficient Anti-Tumor Therapy

ZhiFeng Chen[1,2], WenLing Liu[2], ZiJian Zeng[2], ZhiHong Yan[3,4], LiHeng Ma[1], Yi Liu[1–4], XianShuo Cao[2]

[1]Department of Radiology, The First Affiliated Hospital of Guangdong Pharmaceutical University, Guangzhou, 510080, People's Republic of China; [2]School of Chemistry and Chemical Engineering, Guangdong Pharmaceutical University, Zhongshan, 528458, People's Republic of China; [3]School of Pharmacy, Guangdong Pharmaceutical University, Guangzhou, 510006, People's Republic of China; [4]Guangdong B. C. Biotech Co., Ltd, Zhongshan, 528007, People's Republic of China

Correspondence: Yi Liu; XianShuo Cao, School of Chemistry and Chemical Engineering, Guangdong Pharmaceutical University, Zhongshan, 528458, People's Republic of China, Email liuyi_papers@163.com; caoxianshuo@gdpu.edu.cn



**Purpose:** This study designed a dopamine derivative integrating active targeting and pH-responsive borate ester bond-mediated passive targeting to construct drug delivery systems for tumor-targeted drug delivery, thus improving antitumor drug bioavailability and expanding the application of dopamine in drug delivery.

**Methods:** Nuclear magnetic resonance and Fourier transform infrared spectrometry were used to determine the structures of Man-PBA-DAO and Man-2PBA-DAO. Hydrodynamic diameter measurements confirmed the pH responsiveness of the targeting nanoparticles in different pH media over 12 hours. Nanoparticle toxicity was assessed using the MTT assay. Cellular uptake of the targeting nanoparticles was evaluated using flow cytometry and fluorescence microscopy. High-performance liquid chromatography (HPLC) was employed to quantify curcumin content.

**Results:** Covalent binding of mannose molecules to the dopamine derivative molecule allowed it to specifically target A549 cells with mannose receptors. More importantly, a significantly accelerated drug release (about 62% at pH=5.0) at low pH values was achieved by regulating the number of acidic-responsive borate bonds in polymer main chains. As a result, due to active targeting of mannose and passive targeting of acid response, Curcumin-loaded nanoparticles offer remarkably enhanced inhibiting efficiency against A549 cells at a low concentration of 6.25 μg/mL.

**Conclusion:** The dopamine derivative Man-2PBA-DAO-constructed dual active-passive targeting nano micelles enabled precise delivery and controllable release of Cur, offering new prospects for dopamine-based drug delivery in lung cancer treatment.

**Keywords:** dopamine derivatives, micelle nanoparticles, dual-target, curcumin

## Introduction

Lung cancer is one of the most commonly diagnosed cancers, with 2 million new cases and 1.79 million deaths each year.[1] Currently, chemotherapy still remains the mainstay for lung cancer due to its high therapeutic efficacy. Despite a variety of anti-tumor active pharmaceutical ingredients that have been discovered, such as curcumin (Cur), doxorubicin (DOX) hydrochloride, methotrexate (MTX) and paclitaxel (PTX), many of them face the limitations of low solubility, poor specificity and systemic toxicities.[2–5] These issues lead to low bioavailability, a lack of specific recognition between tumor tissue and normal tissue, and ultimately to acute deterioration of patients' health.[6] Therefore, it is urgent to develop new strategies to enhance therapeutic efficacy.

Received: 10 April 2025
Accepted: 29 July 2025
Published: 20 August 2025

**Graphical Abstract**

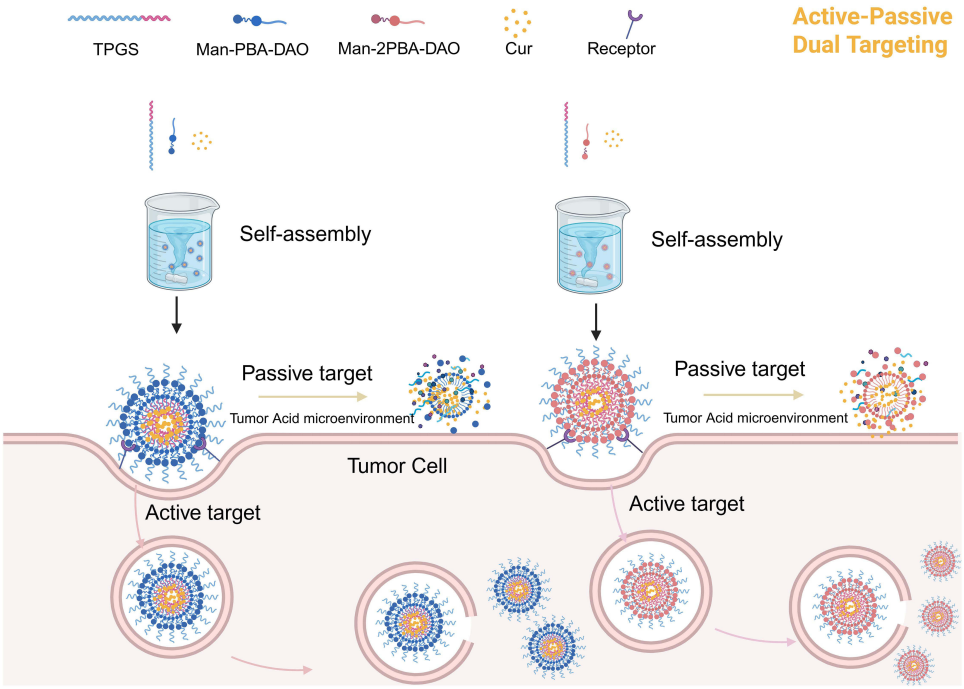


The development of drug delivery systems has provided an effective approach to overcome the aforementioned drawbacks of chemotherapy drugs.[7,8] Among them, polymeric nanoparticles have attracted continuing interest. These nanoparticles not only enhance drug solubility and thus improve bioavailability, but also control the release rate by modulating the degradation rate, thus reducing toxic side effects. Various polymeric nanocarriers have been developed in recent years, of which the most commonly studied is polydopamine (PDA), integrating numerous advantages including ease of preparation, excellent biocompatibility and abundance of functional groups that can be anchored to drug molecules.[9–14] For example, Yan et al prepared Cur-loaded polydopamine nanoparticles with a particle size of about 180 nm, which released 40% at 16 h, and MCF-7 cells incubated with their nanoparticles showed 40% viability.[15] Another example is the work by Yanyan Zhang et al, who developed a multifunctional nanoplatform loaded with Cisplatin (CP), featuring a particle size of approximately 198 nm. The CP Drug Loading Capacity (DLC) and Encapsulation Efficiency (EE) were 15.8±0.1% and 18.7±0.2%, respectively. At a CP concentration of 30 μg/mL, the nanoparticles induced about 50% cell death.[16] However, depending only on polymer disintegration to control drug release is inadequate for achieving the optimal release rate. Also, the particle size of these nanoparticles is difficult to regulate, which hinders their delivery to the tumor site through the enhanced permeability and retention (EPR) effect.[17] Therefore, achieving polymeric nanoparticles with targeted drug delivery coupled with rapid drug release in tumor cells and controllable particle size is a crucial consideration for enhancing drug delivery efficiency.

Polymeric micelles have emerged as biocompatible carriers for drug delivery.[18–20] Compared to polydopamine nanoparticles, polymeric micelle nanoparticles offer several advantages. Firstly, these micelle nanoparticles can achieve very small particle sizes (between 10 and 100 nm) by readily altering the ratio of amphiphilic molecules in the system, allowing for passive targeting to tumor tissues through the EPR effect.[21–23] Secondly, amphiphilic molecules can specifically target drugs to tumor tissue by anchoring tumor-targeting ligands on the surface of micelle nanoparticles.[24,25] Moreover, these micelles can offer controlled drug release in a specific tumor microenvironment when constructed using stimuli-sensitive amphiphilic molecules.[26,27] Currently, various amphiphilic molecules including D-α-tocopherol polyethylene glycol 1000 succinate (TPGS), polyethylene glycol-

polylactide (PEG-PLA) and Pluronic F-127 have been used to prepare micelles.[28,29] To our knowledge, there are few reports on micelles using dopamine molecules as micellar molecules.

Herein, a new type of micellar nanoparticle was developed based on pH-responsive and active-targeting dopamine derivatives for lung cancer therapy. In detail, mannose (Man) was linked to linoleic acid (DAO) via pH-responsive borate ester bonds to form amphiphilic dopamine derivatives, which were then self-assembled with TPGS and Cur to prepare micellar nanoparticles with controlled size, pH-responsive and active-targeting properties. We hypothesize that the mannose decoration enables an active targeting-delivery to tumor cells overexpressing mannose receptors, while pH-sensitivity allows a rapid intracellular release of the loaded Cur in response to the acidic environment. As expected, the in vitro results demonstrated significant tumor cell inhibition efficacy and excellent cellular uptake. This design strategy is expected to pave the way for dopamine-derived molecules in lung cancer drug delivery.

# Materials and Methods

## Materials Cell and Instruments

Mannose and mannosamine were purchased from Shanghai Aladdin Biochemical Technology Co., Ltd. Dopamine hydrochloride, linoleic acid, 1,4-phenylenebisboronic acid, and 4-carboxyphenylboronic acid were obtained from Shanghai Macklin Biochemical Technology Co., Ltd. Pyrene, TPGS, methanol, 1-ethyl-(3-dimethylaminopropyl) carbodiimide hydrochloride (EDC), 1-hydroxybenzotriazole (HOBt), and *N, N*-dimethylformamide (DMF) were purchased from Meryer (Shanghai) Chemical Technology Co., Ltd. The MTT kit was obtained from Beijing Solarbio Science & Technology Co., Ltd. A549 and HaCaT cells were obtained from Bohui Biological Technology Co., Ltd. (Guangzhou, China).

Malvern Particle Size Analyzer (ZetasizerNanoZS90, Malvern, UK), Nuclear Magnetic Resonance Spectrometer (NMR, AVANCE III HD 400, Bruker, Germany), Fourier Transform Infrared Spectrometer (FT-IR, Nicolet iS50 FT-IR Spec, Thermo Scientific, USA), Transmission Electron Microscope (TEM, Talos F200×, FEI, USA), High Performance Liquid Chromatography (HPLC, ultimate 3000, Thermo Scientific, USA) Flow cytometer (CytoFLEX, Beckman Coulter, USA) Fluorescent inverted microscope. (Ckx41, Olympus Corporation, JP).

## Synthesis of DAO, Man-PBA-DAO and Man-2PBA-DAO

DAO synthesis:[30] Linoleic acid (1 mmol), 1-ethyl-(3-dimethylaminopropyl) carbodiimide hydrochloride (EDC, 1 mmol), and 1-hydroxybenzotriazole (HOBt, 1 mmol) were dissolved in N, N-dimethylformamide (DMF, 5 mL). The mixture was stirred at 1000 rpm at 0 °C for 40 min and at room temperature for 120 min, sequentially. Dopamine hydrochloride (1 mmol) and triethylamine (3 mmol) were then added, followed by stirring at 1000 rpm (room temperature, 14 h). The dopamine derivative DAO was isolated by column chromatography.

Man-PBA-DAO synthesis: DAO (1 mmol) and 4-carboxyphenylboronic acid (1 mmol) were dissolved in DMF (5 mL). After adding triethylamine (1 mmol), the reaction proceeded for 6 h. Mannosamine hydrochloride (1 mmol) was subsequently coupled via amination to afford the amphiphilic derivative Man-PBA-DAO.

Man-2PBA-DAO synthesis: A mixture of D-mannose (1 mmol), 1,4-phenylenebisboronic acid (1 mmol), and triethylamine (1 mmol) in methanol (5 mL) was stirred at 1000 rpm (room temperature, 6 h). The intermediate product was combined with DAO (1 mmol) and additional triethylamine (1 mmol), stirred for 6 h, then concentrated. Man-2PBA-DAO was purified by flash chromatography (eluent: $CH_2Cl_2$/MeOH = 50:3, v/v).

## Preparation of Nanoparticles

### Preparation of TPGS/Man-PBA-DAO and TPGS/Man-2PBA-DAO Nanoparticles

Solutions of TPGS, Man-PBA-DAO, and Man-2PBA-DAO (1 mg/mL in methanol) were prepared. These solutions were mixed at specified ratios (Tables S2 and S3), followed by evaporation to dryness. The residue was reconstituted in 5 mL water, then vortex-mixed and sonicated to obtain nanoparticle solution.

### Preparation of TPGS/Man-PBA-DAO/Cur and TPGS/Man-2PBA-DAO/Cur Drug-Loaded Nanoparticles

A methanol solution of Cur (1 mg/mL, 0.1 mL) was mixed with TPGS/Man-PBA-DAO (1:0.1, w/w) and TPGS/Man-2PBA-DAO (1:0.75, w/w), respectively. Following solvent removal, the residue was reconstituted in 5 mL deionized water, then vortex-mixed and sonicated to obtain drug-loaded nanoparticle solution.

## Characterization and Performance Evaluation of Nanoparticles

### Ultraviolet Spectroscopic Determination

Solutions of TPGS (1mg/mL), TPGS/Man-PBA-DAO (1:0.1, w/w), TPGS/Man-2PBA-DAO (1:0.75, w/w), TPGS/Man-PBA-DAO/Cur (1:0.1:0.1, w/w/w), and TPGS/Man-2PBA-DAO/Cur (1:0.75:0.1, w/w/w) were prepared. Their UV absorption spectra were measured using an ultraviolet spectrophotometer with a scanning range of 200–400 nm.

### TPGS/Man-PBA-DAO/Cur and TPGS/Man-2PBA-DAO/Cur Nanoparticles TEM

A drug-loaded nanoparticle aqueous solution was prepared and diluted 100-fold. A droplet of the diluted solution was deposited onto an ultrathin carbon support film and allowed to adsorb for 15 min. The sample was then negatively stained with 1% phosphotungstic acid (PTA) solution and dried under infrared light.

### The Particle Size Distribution of TPGS/Man-PBA-DAO and TPGS/Man-2PBA-DAO Nanoparticles Before and After Drug Loading

Solutions of TPGS, TPGS/Man-PBA-DAO (1:0.1, w/w), TPGS/Man-2PBA-DAO (1:0.75, w/w), TPGS/Man-PBA-DAO /Cur (1:0.1:0.1, w/w/w), and TPGS/Man-2PBA-DAO/Cur (1:0.75:0.1, w/w/w) were prepared at specific concentrations, and their particle size distributions were measured using a Malvern particle size analyzer.

### CAC Determination of TPGS/Man-PBA-DAO and TPGS/Man-2PBA-DAO Nanoparticles

Two nanoparticle solutions were prepared at 12 concentrations ranging from 0.00175 to 0.14 μg/mL. For each concentration, 10 mL of the solution was added to a headspace bottle containing 0.12 μg of pyrene. The mixtures were heated at 40 °C for 90 min. Fluorescence spectra were recorded with an excitation wavelength of 335 nm and an emission wavelength range of 350–450 nm. Both excitation and emission slit widths were set to 5 nm. The CAC value was determined by plotting the fluorescence intensity against the negative logarithm of the nanoparticle concentration.

### Evaluation of pH Responsiveness of TPGS/Man-PBA-DAO and TPGS/Man-2PBA-DAO Nanoparticles

The two nanoparticle stock solutions were incubated in HCl solution (pH 1.5) and PBS buffers (pH 5.0, 6.8, 7.4, and 9.5) for 24 h, respectively. Their particle sizes were then measured using a Malvern particle size analyzer.

### Measurement of Encapsulation Efficiency and Drug Loading Capacity of Drug-Loaded Nanoparticles

The encapsulation efficiency (EE) and drug loading capacity (DLC) of TPGS/Man-PBA-DAO and TPGS/Man-2PBA-DAO nanoparticles were quantitatively analyzed by high-performance liquid chromatography (HPLC). Specifically, two aliquots of nanoparticle solutions were prepared. For the first aliquot, after centrifugation (7000 rpm, 20 min), the supernatant (1 mL) was mixed with methanol (4 mL) to obtain Solution 1. For the second aliquot, 1 mL of the uncentrifuged sample was directly mixed with methanol (4 mL) to obtain Solution 2. The Cur concentration was determined using a standard curve (Figure S6). The chromatograms of Cur and nanoparticles are presented in Figure S5, and the chromatographic conditions are described in the Supplementary Materials. Equations (1) and (2) were used to calculate EE and DLC.

$$EE(\%) = \frac{W_{Loaded\ Drug}}{W_{Total\ Drug}} \times 100\%\# \tag{1}$$

$$DLC(\%) = \frac{W_{Loaded\ Drug}}{W_{Drug\ Loaded\ Nanoparticles}} \times 100\%\# \tag{2}$$

Among them, $W_{\text{Loaded Drug}}$ represents the content of the drug encapsulated in the nanoparticles, $W_{\text{Total Drug}}$ represents the total amount of drug added in the preparation of drug-loaded nanoparticles, and the $W_{\text{Drug Loaded Nanoparticles}}$ represents the drug content in the nanoparticles and the total amount of the carrier.

### In vitro Drug Release Curve Test

TPGS/Man-PBA-DAO and TPGS/Man-2PBA-DAO nanoparticle solutions (5 mL each) were loaded into 3.5 kDa dialysis bags (10 cm length). After sealing both ends, the bags were immersed in 20 mL PBS buffers (pH 7.4, 6.8, or 5.0; each containing 0.5% Tween 80) and incubated at 37°C. At 0.5, 1, 2, 3, 4, 6, 8, 10, 12, 24, 36, and 72 h, 1 mL aliquots were withdrawn and replaced with fresh medium. Curcumin content was quantified by HPLC, and cumulative release was calculated using equation (3).

$$Cumulativerelease(\%) = \frac{20 \times C_n + \sum_{i=1}^{n-1} C_i \times 1}{TheamountofCurinnanoparticlessolutions} \times 100\% \quad (3)$$

### MTT Cytotoxicity and Live/Dead Staining Test

A549 or HaCaT cells in the logarithmic growth phase were seeded in 96-well plates ($1\times10^4$ cells/well) and incubated overnight to allow adherence. After treatment with varying sample concentrations for 72 h, 10% MTT solution in complete medium was added to each well (100 μL/well) and incubated for 4 h. The supernatant was removed, and 110 μL DMSO was added to dissolve formazan crystals. Absorbance was measured at 490 nm, and cell viability was calculated using equations (4).

$$Viability(\%) = \frac{OD_{Sample} - OD_{Blank}}{OD_{Control} - OD_{Blank}} \times 100\%\# \quad (4)$$

### Targeting Evaluation of Nanoparticles

Following the preparation method for curcumin-loaded TPGS/Man-PBA-DAO and TPGS/Man-2PBA-DAO nanoparticles, coumarin-6 (C6) was substituted for curcumin to prepare C6-loaded nanoparticles. The nanoparticles were dispersed in complete medium and added to the cells at a final concentration of 10 μg/mL C6. After incubation, cellular uptake was assessed by fluorescence microscopy imaging and quantified by flow cytometry.

### Statistical Analysis

All data are presented as mean ± standard deviation (SD). Statistical significance was set to $p < 0.05$, and the p-value was expressed by asterisk as follows: * $p < 0.05$, ** $p < 0.01$, *** $p < 0.001$, **** $p < 0.0001$; ns, no significance calculated by unpaired two-tailed *t* test.

## Results and Discussion

### FT-IR and $^1$H-NMR Spectra of Man-PBA-DAO and Man-2PBA-DAO Were Analyzed

According to the synthesis route shown in Figure S1, DAO, Man-PBA-DAO, and Man-2PBA-DAO were synthesized. Successful synthesis was confirmed by FT-IR and $^1$H-NMR. In Figure 1a, a characteristic peak at 3283 $cm^{-1}$ is observed, which is attributed to the stretching vibration of O-H of Man. These peaks at 2856, 2923 and 3015 $cm^{-1}$ are ascribed to C-H stretching vibrations ($sp^3$ and $sp^2$ hybridized carbon). The C=O stretching vibration peak at 1730 $cm^{-1}$ can be attributed to the formation of diquinone, resulting from the oxidation of unstable o-diphenol hydroxyl groups in DAO.[31,32] The disappearance of the peak at 1730 $cm^{-1}$ demonstrates the formation of boronic ester bonds, confirming the successful synthesis of Man-2PBA-DAO.[33] Similar peaks are also observed in the Man-PBA-DAO sample (Figure 1b) except for a new C-N stretching vibrational peak at 1570 $cm^{-1}$ belonging to the amide bonds. Meanwhile, the preparation of samples was also validated by $^1$H-NMR spectra. As shown in Figure 1c and d, all peaks of the two samples are fully assigned, which further supports the successful synthesis of Man-2PBA-DAO and Man-PBA-DAO.

### Preparation and Characterization of Drug-Loaded Nanoparticles

The nanoparticles were fabricated through the self-assembly of TPGS and rationally designed dopamine derivative (Figure 2a). The size of nanoparticles can be regulated by adjusting the ratio of TPGS to Man-PBA-DAO or Man-2PBA-DAO. From Table S2 and S3, the particle size exhibits a content-dependent increase with elevated contents of both Man-PBA-DAO and Man-2PBA-DAO, reaching minimal values (62.34 ± 9.236 nm and 119.9 ± 3.318 nm) at 0.10 mg and

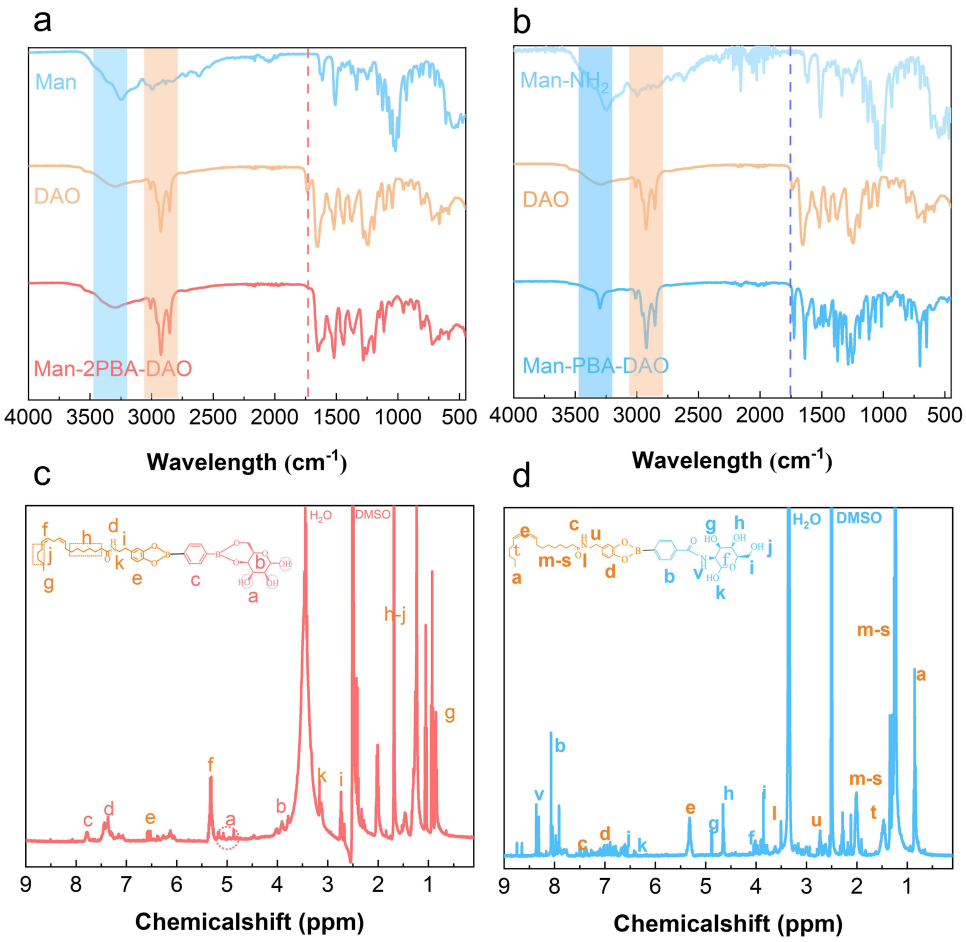


**Figure 1** (**a**)Man-2PBA-DAO and (**b**) Man-PBA-DAO, NMR hydrogen spectra of (**c**) Man-2PBA-DAO and (**d**) Man-PBA-DAO.

0.75 mg, respectively. The gradual expansion of the hydrophobic core results in the increase of particle size.[34] The particle size was also measured by TEM. As shown in Figure 2b and c, the nanoparticles exhibit uniform spherical morphology with particle sizes below 100 nm.

As shown in Figure 2d and e, the UV-Vis spectrum of TPGS exhibits a characteristic absorption peak at 279–290 nm, attributed to the π→π* transition. With the addition of Man-PBA-DAO and Cur, the absorption peak broadens and undergoes a red-shift, which is more pronounced in the nanoparticles prepared from TPGS/Man-PBA-DAO, suggesting the presence of π-π interactions.[35,36]

According to Figure 2f and g, both nanoparticles demonstrate a significant reduction in particle size as measured by Dynamic Light Scattering (DLS), attributed to the enhanced π-π stacking interactions between the hydrophobic regions of TPGS, Man-PBA-DAO (or Man-2PBA-DAO) and Cur, which leads to closer molecular packing and consequently results in decreased particle size.[37]

Furthermore, the π-π interactions are substantiated by the experimental results presented in Figure 2h and i. Comparative analysis reveals significant differences in drug loading capacity (DLC) between TPGS/Man-2PBA-DAO /Cur and TPGS/Man-PBA-DAO/Cur nanoparticles. Specifically, at a curcumin (Cur) content of 600 μg, the Man-2PBA-DAO-based nanoparticles achieve a DLC exceeding 20%. The increased loading capacity can be attributed to the existence of p-π conjugation in 1,4-benzenediboronic acid, which endows Man-2PBA-DAO with an extended π-electron cloud to support robust π-π stacking interactions between the carrier and drug molecules.[38–42]

The stability of the composite nanoparticles was evaluated by determining their critical aggregation concentration (CAC; the minimal concentration of the amphiphilic components required for self-assembly, eg, TPGS/Man-nPBA-DAO, n = 1, 2).[43] As shown in Figure S4, the CAC1 and CAC2 values of the Man-PBA-DAO nanoparticles and Man-2PBA-DAO nanoparticles are

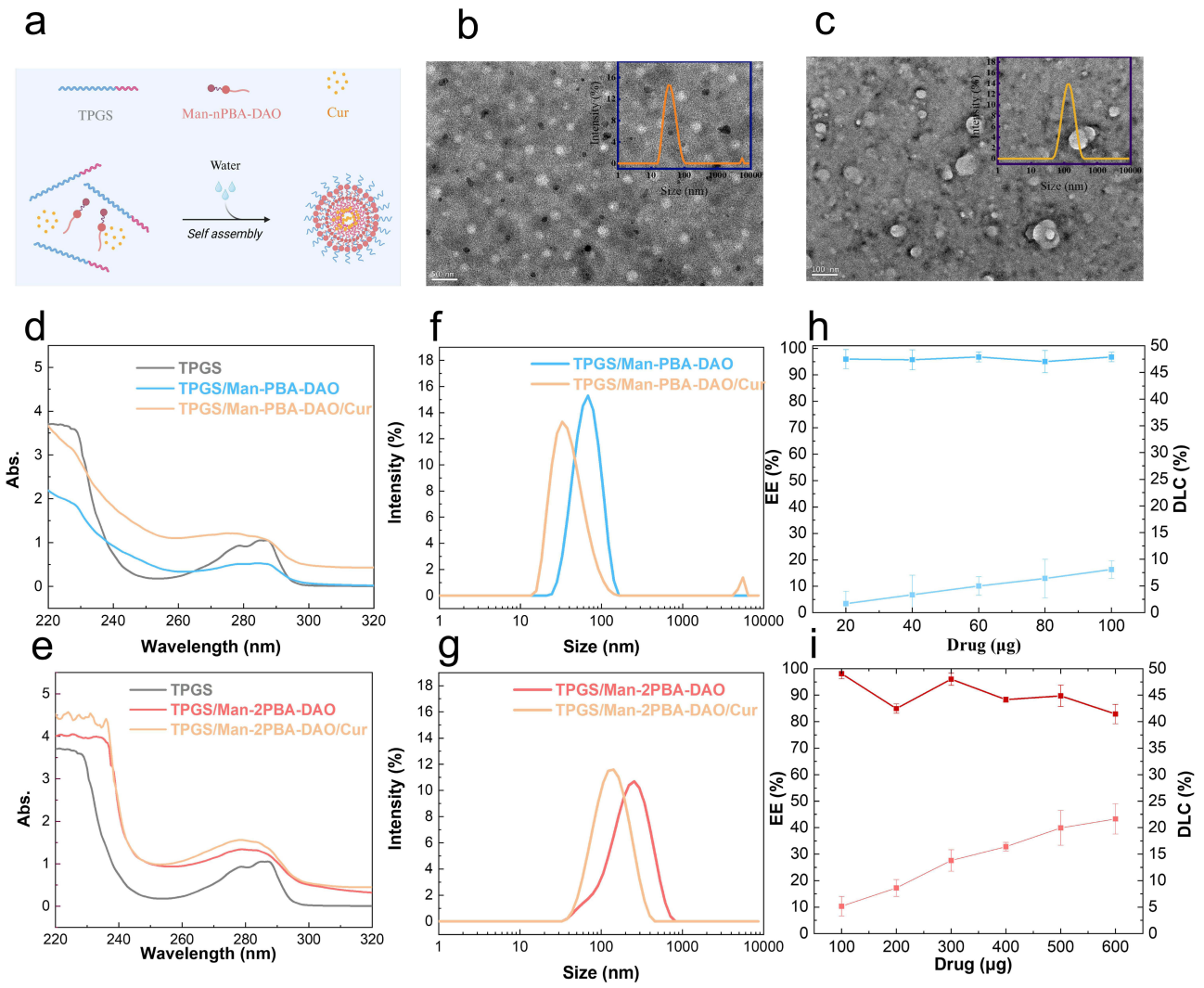


**Figure 2** (**a**) Schematic diagram of nanoparticle self-assembly. The TEM of TPGS/Man-PBA-DAO/Cur (**b**) and TPGS/Man-2PBA-DAO/Cur (**c**) nanoparticles. The UV spectra of nanoparticles constructed with two dopamine derivatives Man-PBA-DAO (**d**) and Man-2PBA-DAO (**e**). The particle size distribution of TPGS/Man-PBA-DAO (**f**) and TPGS/Man-2PBA-DAO (**g**) nanoparticles before and after drug loading. Encapsulation efficiency and drug loaded nanoparticles TPGS/Man-PBA-DAO/Cur (**h**) and TPGS/Man-2PBA-DAO/Cur (**i**). Results are presented as mean ± SD, n = 3 independent samples.

measured to be 0.0008 mg/mL and 0.2605 μg/mL, significantly lower than the critical micelle concentration CMC of TPGS (0.2 mg/mL).[44] This substantial difference indicates that the incorporation of Man-PBA-DAO significantly enhances the dilution stability of nanoparticles, enabling them to maintain structural integrity even at low concentrations without disintegration.[45]

## pH Response Performance of Nanoparticles and Cumulative Release Curve of Drug-Loaded Nanoparticles

As shown in Figure 3a, owing to the boronic ester bond, the nanoparticles are anticipated to exhibit an increase in particle size as pH decreases, specifically in Figure 3b and c, at pH values of 6.8, 5.0, and 1.5, the nanoparticles exhibit broadened size distributions and increased hydrodynamic diameters, confirming acid-responsive behavior.[46] Also, the nanoparticles display acid-dependent release properties, as evidenced in Figure 3d and e, with significantly higher cumulative release rates observed under acidic conditions, primarily due to $H^+$ attacking the boronic ester bond, forming a tetrahedral intermediate that undergoes hydrolysis. This leads to bond cleavage and partial detachment of mannose-phenylboronic acid conjugates from the nanoparticles. Consequently, the increased proportion of hydrophobic segments destabilizes the nanoparticles, accelerating Cur release.[47–51] Remarkably, the Man-2PBA-DAO-based drug-loaded nanoparticles demonstrate superior pH-responsive drug


https://doi.org/10.2147/IJN.S528334

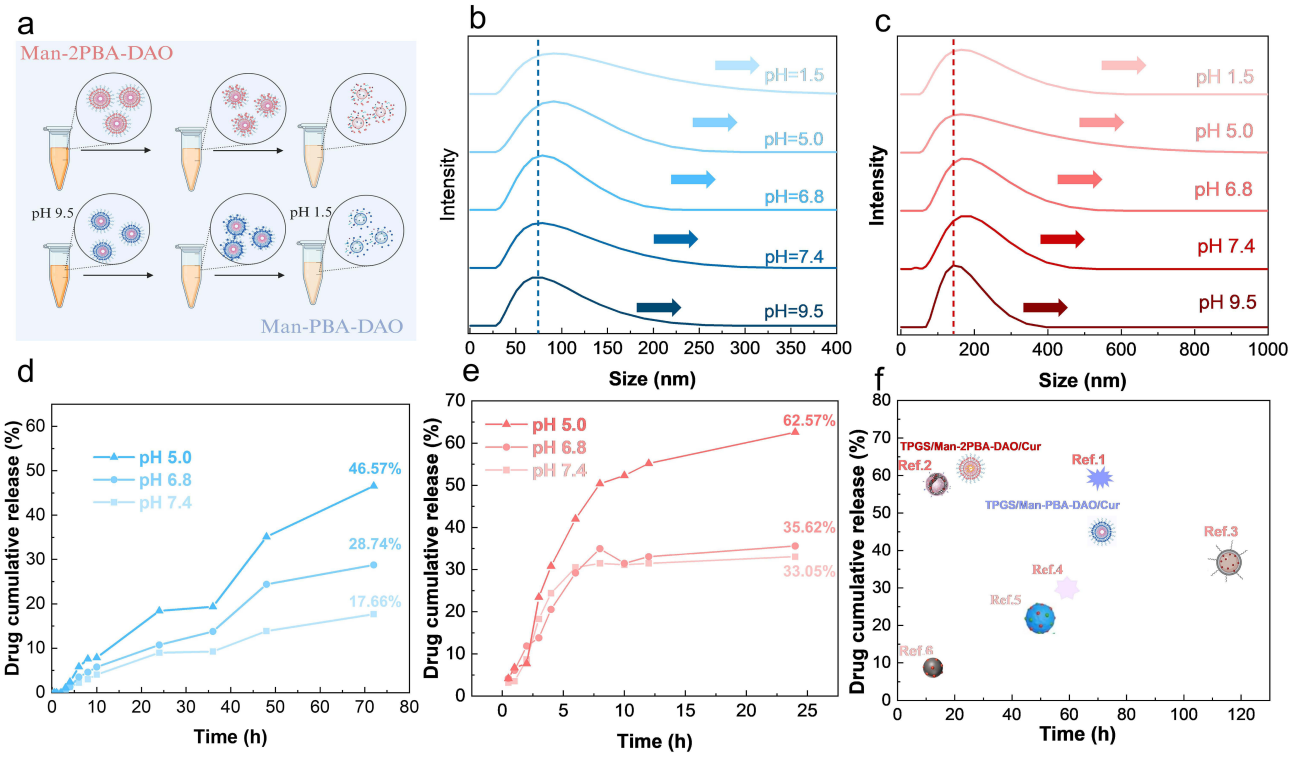


**Figure 3** (**a**) Dissociation of nanoparticles as pH decreases. (**b**) TPGS/Man-PBA-DAO and (**c**) TPGS/Man-2PBA-DAO size distribution in PBS at varying pH. (**d**) TPGS/Man-PBA-DAO/Cur and (**e**) TPGS/Man-2PBA-DAO/Cur cumulative drug release. (**f**) Comparison of drug release between nanoparticles in this study and polydopamine nanoparticles. Ref.1.[53] Ref.2[54] Ref.3[55] Ref.4[14] Ref.5[56] Ref.6.[57]

release properties compared to the Man-PBA-DAO-based ones. Specifically, the TPGS/Man-2PBA-DAO/Cur nanoparticles achieve nearly 62% drug release within 24 h, whereas the TPGS/Man-PBA-DAO/Cur nanoparticles release only 50%, even when extended to 72 h. This difference is attributed to the higher probability of cleavage of dual boronic ester bonds in the former, which enable accelerated drug release from nanoparticles.[52] Additionally, it is worth noting that the drug release capability of TPGS/Man-2PBA-DAO/Cur is comparable to and even outstrips previously reported dopamine carriers (Figure 3f).

## The Effect of Drug-Loaded Nanoparticles on A549 and HaCaT Cells

As shown in Figure 4a, the concentrations of Cur up to 25 μg/mL in both nanoparticles show no significant reduction in HaCaT cell viability, indicating biocompatibility. We then evaluated the in vitro antitumor efficacy of two drug-loaded nanoparticles. As shown in Figure 4b, at a concentration of 6.25 μg/mL, the antitumor efficacy of the two targeted nanoparticles is nearly 9-fold higher than free Cur. At 1.5625 μg/mL, TPGS/Man-2PBA-DAO/Cur shows significantly enhanced cytotoxicity against A549 cells compared to TPGS/Man-PBA-DAO/Cur ($P < 0.1$), which is attributed to cleavage of dual boronic ester bonds.

## Qualitative Analysis of Nanoparticle Targeting Evaluation

The cellular uptake of TPGS/Man-PBA-DAO and TPGS/Man-2PBA-DAO nanoparticles was evaluated in A549 and HaCaT cells using coumarin-6 (C6)-labeled nanoparticles. As shown in Figure 5a, A549 cells exhibited significantly stronger green fluorescence than HaCaT cells. The significant fluorescence difference in different cell lines indicates the targeting specificity of micelle nanoparticles towards A549 cells, which is attributed to the dual-targeting activity through mannose receptor-mediated active targeting and pH-mediated passive targeting. Also, similar observations are obtained from flow cytometry analysis. Flow cytometry analysis corroborated these findings (Figure 5b–d). Notably, A549 cells treated with TPGS/Man-2PBA-DAO/C6 nanoparticles exhibited higher fluorescence intensity than those treated with TPGS/Man-PBA-DAO/C6 nanoparticles. This enhancement is attributed to improved pH-responsive drug release from

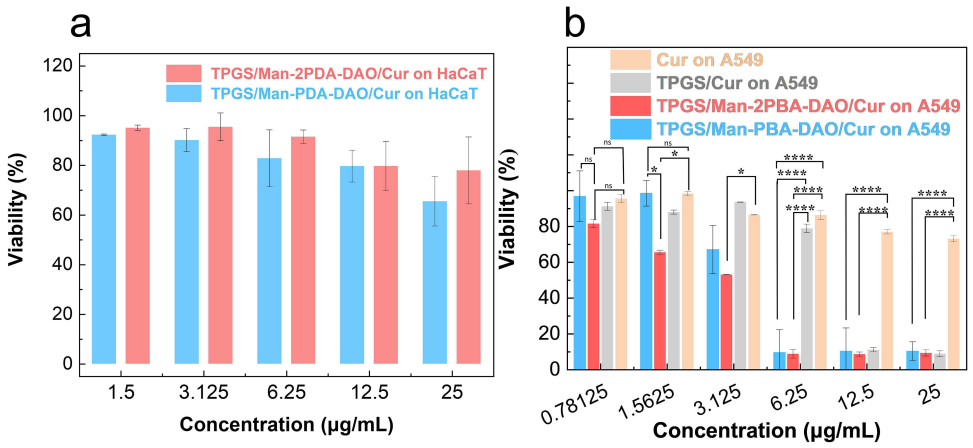


**Figure 4** (**a**) The cytotoxicity of TPGS/Man-PBA-DAO/Cur and TPGS/Man-2PBA-DAO/Cur against HaCaT. (**b**) The cytotoxicity of TPGS/Man-PBA-DAO/Cur, TPGS/Man-2PBA-DAO/Cur, TPGS/Cur and Cur against A549. Data are presented as mean ± SD, n = 3 independent samples. ns, not significant; *, P < 0.1; ****, P < 0.0001.

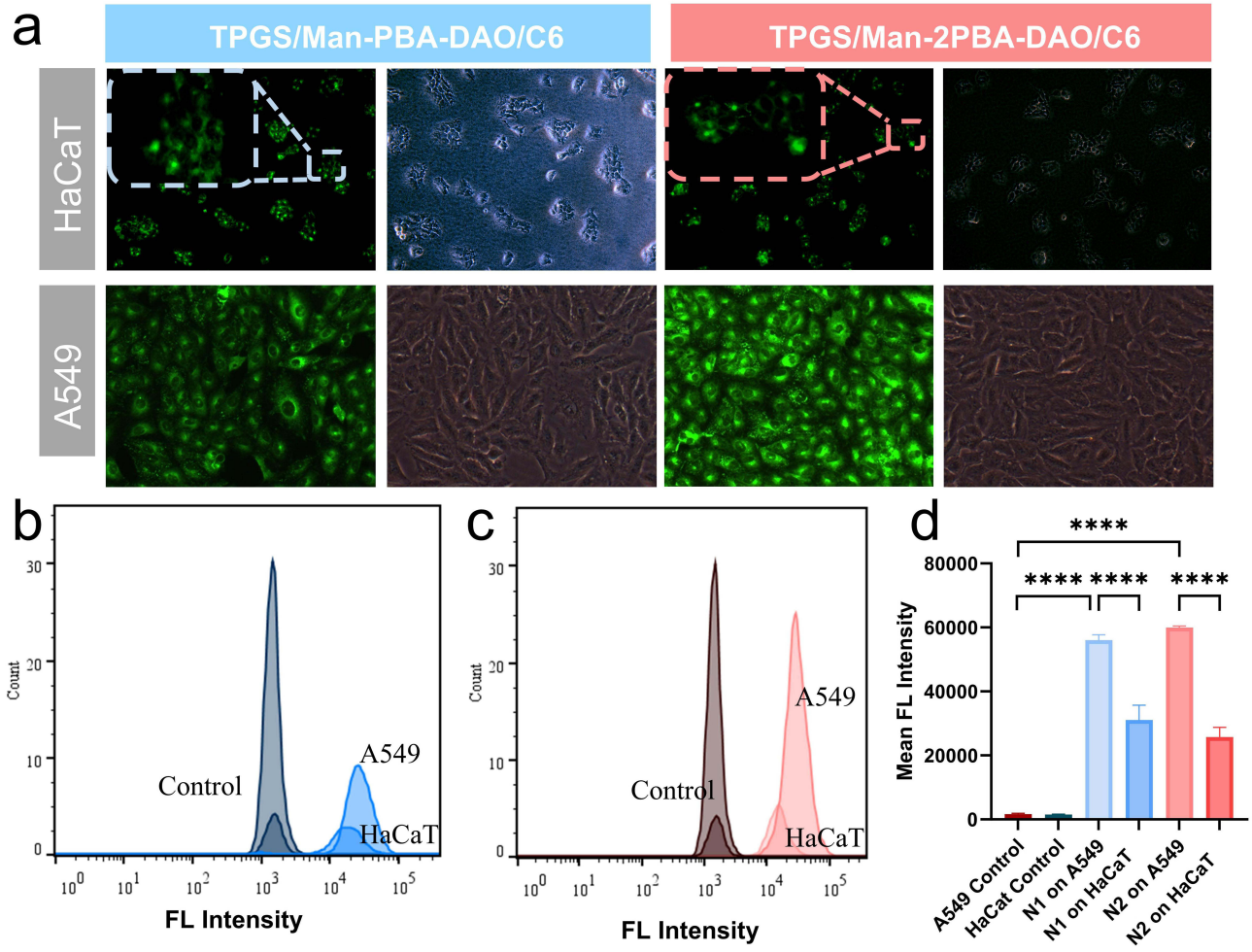


**Figure 5** (**a**) The phagocytosis of two types of nanoparticles by A549 and HaCaT cells (×200). The uptake of two C6-containing nanoparticles (**b**) TPGS/Man-PBA-DAO/C6 and (**c**) TPGS/Man-2PBA-DAO/C6 by A549 cells and HaCaT cells. (**d**) The analysis of Mean FL Intensity of TPGS/Man-PBA-DAO/C6 (N1) and TPGS/Man-2PBA-DAO /C6 (N2). Data are presented as mean ± SD, n =3 independent samples. ****, P < 0.0001.


https://doi.org/10.2147/IJN.S528334

the dual boronic ester bonds in Man-2PBA-DAO.[58,59] These results indicate that dual-targeting plays a critical role in nanoparticle uptake, enhancing anticancer drug accumulation in tumor cells.[58,60,61]

## Conclusion

In summary, we use dopamine derivatives (Man-nPBA-DAO) as amphiphilic molecules to fabricate micelle nanoparticles with controlled size and active-passive targeting activity. The hydrophobic drug Cur is encapsulated in micelles and drug loading capacity could be increased 20% by regulating π-π stacking interactions between the carriers and drug molecules. Owing to overexpressed mannose receptors on tumor cells, the drug-loaded micelles are able to successfully enter the cancer cells. Moreover, the drug encapsulated in the Man-2PBA-DAO micelles is rapidly released from the carriers, resulting in an excellent killing effect on tumor cells at a low concentration of 6.25 μg/mL. This accelerated release can be attributed to rapid micellar depolymerization caused by the disruption of more boronate ester bonds on the Man-2PBA-DAO micelles by intracellular low pH. Meanwhile, the Cur-loaded micelle shows excellent safety for normal cells. This work highlights a well-designed strategy to construct dual-targeting nanoparticles, bringing new prospects for clinical translation in the dopamine-based drug delivery field for lung cancer therapy.

## Declaration of Generative AI and AI-Assisted Technologies in the Writing Process

During the preparation of this work the author(s) used Deepseek in order to improve language and readability. After using this tool, the authors reviewed and edited the content as needed and take full responsibility for the content of the publication.

## Funding

This work was supported by the Guangdong Pharmaceutical University & Shenzhen Bao`an Songgang People`s Hospital Joint Cultivation and Research Fund Project (SGYY2024A008).

## Disclosure

The author(s) report no conflicts of interest in this work.

## References

1. Thai AA, Solomon BJ, Sequist LV, Gainor JF, Heist RS. Lung cancer. *Lancet*. 2021;398(10299):535–554. doi:10.1016/S0140-6736(21)00312-3
2. Malinovskaya J, Kovshova T, Melnikov P, et al. The second phase of tumor invasion driven by immune cells: a study on doxorubicin-loaded PLG nanoparticles. *J Control Release*. 2025;378:750–762. doi:10.1016/j.jconrel.2024.12.056
3. Guo R, Zhong L, Ma S, et al. A biomimetic solution, albumin–doxorubicin molecular complex, targeting tumor and tumor-draining lymph nodes. 10.1039/D4TB01917B. *J Mat Chem B*. 2024;12(47):12320–12337. doi:10.1039/D4TB01917B
4. Wang MY, Qu Y, Hu DR, et al. Methotrexate-loaded biodegradable polymeric micelles for lymphoma therapy. *Int J Pharm*. 2019;557:74–85. doi:10.1016/j.ijpharm.2018.12.025
5. Lin S, Yu Y, Wu E, et al. Reexamining in vivo fate of paclitaxel-loaded polymeric micelles. *Nano Today*. 2024;56:102255. doi:10.1016/j.nantod.2024.102255
6. Islam KM, Ryan J, Fetrick A, Ganti AK. Late-stage lung cancer patient preferences about chemotherapy treatment adverse side effects. *J Clin Oncol*. 2016;34(3_suppl):93. doi:10.1200/jco.2016.34.3_suppl.93
7. Aminu N, Bello I, Umar NM, Tanko N, Aminu A, Audu MM. The influence of nanoparticulate drug delivery systems in drug therapy. *J Drug Delivery Sci Technol*. 2020;60:101961. doi:10.1016/j.jddst.2020.101961
8. Li Q, Lianghao Y, Shijie G, et al. Self-assembled nanodrug delivery systems for anti-cancer drugs from traditional Chinese medicine. 10.1039/D3BM01451G. *Biomater Sci*. 2024;12(7):1662–1692. doi:10.1039/D3BM01451G
9. Chen R, Wen L, Guo F, He J, Wong KH, Chen M. Glutathione-scavenging natural-derived ferroptotic nano-amplifiers strengthen tumor therapy through aggravating iron overload and lipid peroxidation. *J Control Release*. 2025;379:866–878. doi:10.1016/j.jconrel.2025.01.026
10. Hemmatpour H, De Luca O, Crestani D, et al. New insights in polydopamine formation via surface adsorption. *Nat Commun*. 2023;14(1):664. doi:10.1038/s41467-023-36303-8
11. Zhang Y, Tang S, Feng X, et al. Tumor-targeting gene-photothermal synergistic therapies based on multifunctional polydopamine nanoparticles. *Chem Eng J*. 2023;457:141315. doi:10.1016/j.cej.2023.141315
12. Lee HA, Park E, Lee H. Polydopamine and its derivative surface chemistry in material science: a focused review for studies at KAIST. *Adv Mater*. 2020;32(35):1907505. doi:10.1002/adma.201907505
13. Li H, Yin D, Li W, Tang Q, Zou L, Peng Q. Polydopamine-based nanomaterials and their potentials in advanced drug delivery and therapy. *Colloids Surf B*. 2021;199:111502. doi:10.1016/j.colsurfb.2020.111502

14. Zhu Z, Su M. Polydopamine nanoparticles for combined chemo- and photothermal cancer therapy. *Nanomaterials*. 2017;7(7):160. doi:10.3390/nano7070160
15. Yan S, Liao X, Xiao Q, Huang Q, Huang X. Photostabilities and anti-tumor effects of curcumin and curcumin-loaded polydopamine nanoparticles. 10.1039/D4RA01246A. *RSC Adv*. 2024;14(20):13694–13702. doi:10.1039/D4RA01246A
16. Zhang Y, Williams GR, Wang T, et al. Cisplatin-loaded mesoporous polydopamine nanoparticles capped with MnO2 and coated with platelet membrane provide synergistic anti-tumor therapy. *Int J Pharm*. 2024;656:124093. doi:10.1016/j.ijpharm.2024.124093
17. Fang J, Islam W, Maeda H. Exploiting the dynamics of the EPR effect and strategies to improve the therapeutic effects of nanomedicines by using EPR effect enhancers. *Adv Drug Delivery Rev*. 2020;157:142–160. doi:10.1016/j.addr.2020.06.005
18. Liu Y, Sun Y, Zhang W. Synthesis of stimuli-responsive block copolymers and block copolymer nano-assemblies. *Chin J Chem*. 2022;40(8):965–972. doi:10.1002/cjoc.202100821
19. Assiri AA, Glover K, Mishra D, Waite D, Vora LK, Thakur RRS. Block copolymer micelles as ocular drug delivery systems. *Drug Discovery Today*. 2024;29(8):104098. doi:10.1016/j.drudis.2024.104098
20. Bai X, Kang J, Wei S, et al. A pH responsive nanocomposite for combination sonodynamic-immunotherapy with ferroptosis and calcium ion overload via SLC7A11/ACSL4/LPCAT3 pathway. *Exploration*. 2025;5(1):20240002. doi:10.1002/EXP.20240002
21. Yu B, Sun Y, Xiao P, et al. Size control and biological properties of PAMAM-cored multiarm block copolymers. *ACS Appl Bio Mater*. 2023;6(6):2426–2434. doi:10.1021/acsabm.3c00236
22. Sprouse D, Jiang Y, Laaser JE, Lodge TP, Reineke TM. Tuning cationic block copolymer micelle size by pH and ionic strength. *Biomacromolecules*. 2016;17(9):2849–2859. doi:10.1021/acs.biomac.6b00654
23. Lukáš Petrova S, Jäger A, Pavlova E, et al. Probing the inner structure and dynamics of pH-sensitive block copolymer nanoparticles with nitroxide radicals using scattering and EPR techniques. *Eur Polym J*. 2024;220:113473. doi:10.1016/j.eurpolymj.2024.113473
24. Emamgholizadeh Minaei S, Khoei S, Khoee S, Karimi MR, karimi MR. Tri-block copolymer nanoparticles modified with folic acid for temozolomide delivery in glioblastoma. *Int J Biochem Cell Biol*. 2019;108:72–83. doi:10.1016/j.biocel.2019.01.010
25. Venuta A, Moret F, Dal Poggetto G, et al. Shedding light on surface exposition of poly(ethylene glycol) and folate targeting units on nanoparticles of poly(ε-caprolactone) diblock copolymers: beyond a paradigm. *Eur J Pharm Sci*. 2018;111:177–185. doi:10.1016/j.ejps.2017.09.048
26. Duan Z, Zhang Y, Zhu H, et al. Stimuli-sensitive biodegradable and amphiphilic block copolymer-gemcitabine conjugates self-assemble into a nanoscale vehicle for cancer therapy. *ACS Appl Mater Interfaces*. 2017;9(4):3474–3486. doi:10.1021/acsami.6b15232
27. Bai T, Shao D, Chen J, Li Y, Xu BB, Kong J. pH-responsive dithiomaleimide-amphiphilic block copolymer for drug delivery and cellular imaging. *J Colloid Interface Sci*. 2019;552:439–447. doi:10.1016/j.jcis.2019.05.074
28. Lim PQ, Vaibavi SR, Parikh AN, Venkatraman S, Czarny B. Controlling the morphology of poly(ethylene glycol)-b-poly(lactide) Self-assemblies in solution: interplay of homopolymer additives and kinetic traps. *Nanomaterials*. 2024;14(24):2015. doi:10.3390/nano14242015
29. Juang R-S, Wang K-S, Cheng Y-W, et al. Intelligent and thermo-responsive Au-pluronic® F127 nanocapsules for Raman-enhancing detection of biomolecules. *Spectrochimica Acta Part A*. 2022;279:121475. doi:10.1016/j.saa.2022.121475
30. Yu S, Ye Z, Liu Z, et al. Controlled fabrication of polydopamine nanocapsules via polymerization-induced self-assembly. *Chem Mater*. 2022;34(19):8705–8710. doi:10.1021/acs.chemmater.2c01836
31. Yang X, Niu X, Mo Z, et al. Electrochemical chiral interface based on the Michael addition/Schiff base reaction of polydopamine functionalized reduced graphene oxide. *Electrochim Acta*. 2019;319:705–715. doi:10.1016/j.electacta.2019.07.040
32. Guo Y, Baschieri A, Mollica F, et al. Hydrogen atom transfer from HOO. to ortho-quinones explains the antioxidant activity of polydopamine. *Angew Chem Int Ed*. 2021;60(28):15220–15224. doi:10.1002/anie.202101033
33. Fabre B, Hauquier F. Boronic acid-functionalized oxide-free silicon surfaces for the electrochemical sensing of dopamine. *Langmuir*. 2017;33(35):8693–8699. doi:10.1021/acs.langmuir.7b00699
34. Keshavarzi E, Abareghi M, Mohammadi AA. Modeling the electric double layer at the liposome vesicle via classical density functional theory: solution of poisson's equations for curved membranes. *Langmuir*. 2024;40(12):6149–6162. doi:10.1021/acs.langmuir.3c03258
35. Chen F, Xing Y, Wang Z, Zheng X, Zhang J, Cai K. Nanoscale polydopamine (PDA) meets π–π interactions: an interface-directed coassembly approach for mesoporous nanoparticles. *Langmuir*. 2016;32(46):12119–12128. doi:10.1021/acs.langmuir.6b03294
36. Cheng Q, Hao A, Xing P. Engineering π-conjugation of phenylalanine derivatives for controllable chiral folding and self-assemblies. *ACS Nano*. 2024;18(7):5766–5777. doi:10.1021/acsnano.3c12063
37. Liu H, Gu Y, Dai Y, et al. Pressure-induced blue-shifted and enhanced emission: a cooperative effect between aggregation-induced emission and energy-transfer suppression. *J Am Chem Soc*. 2020;142(3):1153–1158. doi:10.1021/jacs.9b11080
38. Zhang Y, Zhao P, Chen X, et al. Near infrared-activatable methylene blue polypeptide codelivery of the NO prodrug via π–π stacking for cascade reactive oxygen species amplification-mediated photodynamic therapy. *ACS Appl Mater Interfaces*. 2023;15(10):12750–12765. doi:10.1021/acsami.2c21280
39. Suzuki A, Guo X, Lin Z, Yamashita M. Nucleophilic reactivity of the gold atom in a diarylborylgold(i) complex toward polar multiple bonds. 10.1039/D0SC05478J. *Chem Sci*. 2021;12(3):917–928. doi:10.1039/D0SC05478J
40. Meng Q, Wang Y, Rong M, et al. Factors affecting the affinity of boronic acid derivatives to linear polyols: the substituents of boronic acid derivatives and relative position of dihydroxyl group in polyols. *Sep Purif Technol*. 2024;340:126698. doi:10.1016/j.seppur.2024.126698
41. Wei M, Wu Y, Li T, et al. Experimental and theoretical studies on the interaction of dopamine hydrochloride with nicotinic acid. *J Solution Chem*. 2022;51(12):1508–1521. doi:10.1007/s10953-022-01206-7
42. He N, Zhao X, Li Z, et al. Polydopamine enhanced interactions of graphene nanosheets to fabricate graphene/polydopamine aerogels with effectively clear organic pollutants. *Langmuir*. 2024;40(18):9592–9601. doi:10.1021/acs.langmuir.4c00363
43. Ritacco H, Kurlat DH. Critical aggregation concentration in the PAMPS (10%)/DTAB system. *Colloids Surf A*. 2003;218(1):27–45. doi:10.1016/S0927-7757(02)00551-4
44. Tian Q, Shi J, Zhao X, Di D, Deng Y, Song Y. The antitumor efficacy of docetaxel is enhanced by encapsulation in novel amphiphilic polymer cholesterol-coupled tocopheryl polyethylene glycol 1000 succinate micelles. *Drug Delivery Transl Res*. 2017;7(5):642–653. doi:10.1007/s13346-017-0403-6
45. Kim J, Ju J, Kim SD, Shin M. Plant-inspired Pluronic–gallol micelles with low critical micelle concentration, high colloidal stability, and protein affinity. 10.1039/D2BM00630H. *Biomater Sci*. 2022;10(14):3739–3746. doi:10.1039/D2BM00630H

46. Zhang Y-H, Zhang Y-M, Yu J, Wang J, Liu Y. Boronate-crosslinked polysaccharide conjugates for pH-responsive and targeted drug delivery. 10.1039/C8CC09956A. *Chem Commun*. 2019;55(8):1164–1167. doi:10.1039/C8CC09956A
47. Lim C, Shin Y, Lee S, et al. Dynamic drug release state and PEG length in PEGylated liposomal formulations define the distribution and pharmacological performance of drug. *J Drug Delivery Sci Technol*. 2022;76:103825. doi:10.1016/j.jddst.2022.103825
48. Liu S, Ono RJ, Yang C, et al. Dual pH-responsive shell-cleavable polycarbonate micellar nanoparticles for in vivo anticancer drug delivery. *ACS Appl Mater Interfaces*. 2018;10(23):19355–19364. doi:10.1021/acsami.8b01954
49. Zhou W, Li C, Wang Z, Zhang W, Liu J. Factors affecting the stability of drug-loaded polymeric micelles and strategies for improvement. *J Nanopart Res*. 2016;18(9):275. doi:10.1007/s11051-016-3583-y
50. Gao Y-E, Ma X, Hou M, et al. Highly cell-penetrating and ultra-pH-responsive nanoplatform for controlled drug release and enhanced tumor therapy. *Colloids Surf B*. 2017;159:484–492. doi:10.1016/j.colsurfb.2017.08.018
51. Wu W, Yi P, Zhang J, et al. 4/6-Herto-arm and 4/6-mikto-arm star-shaped block polymeric drug-loaded micelles and their pH-responsive controlled release properties: a dissipative particle dynamics simulation. 10.1039/C9CP02411E. *Phys Chem Chem Phys*. 2019;21(27):15222–15232. doi:10.1039/C9CP02411E
52. Kang H, Wei W, Sun L, et al. Modular design and bonding mechanism of internal boron–nitrogen coordinated boronic ester hydrogels with alkaline ph responsiveness and tunable gelation pH. *Chem Mater*. 2023;35(6):2408–2420. doi:10.1021/acs.chemmater.2c03550
53. Wang D, Lu K, Zou G, Wu D, Cheng Y, Sun Y. Attenuating intervertebral disc degeneration through spermidine-delivery nanoplatform based on polydopamine for persistent regulation of oxidative stress. *Int J Biol Macromol*. 2024;274:132881. doi:10.1016/j.ijbiomac.2024.132881
54. Lv L, Cheng H, Wang Z, et al. "Carrier–drug" layer-by-layer hybrid assembly of biocompatible polydopamine nanoparticles to amplify photo-chemotherapy. 10.1039/D2NR03200G. *Nanoscale*. 2022;14(37):13740–13754. doi:10.1039/D2NR03200G
55. Steeves M, Combita D, Whelan W, Ahmed M. Chemotherapeutics-loaded poly(Dopamine) Core-shell nanoparticles for breast cancer treatment. *J Pharmacol Exp Ther*. 2024;390(1):78–87. doi:10.1124/jpet.123.001965
56. Liu TXF, Geng L, He R, et al. Micro-electro nanofibrous dressings based on PVDF-AgNPs as wound healing materials to promote healing in active areas. *Int J Nanomed*. 2025;20:771–789. doi:10.2147/IJN.S506489
57. Chen N, Yao S, Li M, et al. Nonporous versus mesoporous bioinspired polydopamine nanoparticles for skin drug delivery. *Biomacromolecules*. 2023;24(4):1648–1661. doi:10.1021/acs.biomac.2c01431
58. Huang Y, Gao Y, Chen T, et al. Reduction-triggered release of CPT from acid-degradable polymeric prodrug micelles bearing boronate ester bonds with enhanced cellular uptake. *ACS Biomater Sci Eng*. 2017;3(12):3364–3375. doi:10.1021/acsbiomaterials.7b00618
59. Zhao Z-H, Zhao P-C, Zhao Y, Zuo J-L, Li C-H. An underwater long-term strong adhesive based on boronic esters with enhanced hydrolytic stability. *Adv Funct Mater*. 2022;32(26):2201959. doi:10.1002/adfm.202201959
60. Gong H, Hu Y, Chen F, et al. Simple and efficient enrichment and separation of glycoprotein by teamed boronate affinity magnetic carbon nanospheres. *Microchem J*. 2024;207:111998. doi:10.1016/j.microc.2024.111998
61. Gong H, Li S, Cheng Y, Chen F, Chen C, Cai C. Rapid, efficient and highly selective separation and enrichment of glycoprotein by surface-imprinted MOF nanoparticles loaded with high-density boric acid. *Sep Purif Technol*. 2025;354:128911. doi:10.1016/j.seppur.2024.128911